Research Article

SOHAG JOURNAL OF SCIENCES

https://doi.org/10.21608/sjsci.2025.400073.1287

Electrochemical and charge-discharge properties of the electrodeposited cobalt, tungsten, and cobalt-tungsten alloy in an acidic medium

Eman Ragab*, Hoda Abdel Shafy Shilkamy*, Hossnia S.Mohran, Mahmoud Elrouby

Department of Chemistry, Faculty of Science, Sohag University, Sohag 82524, Egypt

*Corresponding emails: eman.ragab@science.sohag.edu.eg,

Received: 2nd July 2025 **Revised:** 4th August 2025 **Accepted:** 25th August 2025
Published online: 8th September 2025

Abstract

This study explores the electrochemical behavior and charge-discharge characteristics of cobalt (Co), tungsten (W), and Co–W alloy coatings electrodeposited onto copper substrates. The investigations were carried out at 25 °C in 0.1 M H_2SO_4 aqueous solution. The specific capacitance of each electrode was determined under identical conditions to evaluate and compare their electrochemical performance. Among the three types of coatings, pure cobalt prepared using the chronoamperometric method exhibited superior specific capacitance and enhanced charge-discharge behavior in the acidic environment. These results suggest that Co coatings are more effective in storing and delivering charge under the studied conditions. In contrast, tungsten coatings demonstrated a higher specific energy density compared to both pure Co and Co–W alloy coatings, indicating their potential advantage in applications requiring greater energy output. The comparative analysis highlights the influence of composition and structure on the electrochemical efficiency of the coatings, offering insights into the design of advanced electrode materials for energy storage systems.

Keywords: Co-W alloy, electrodeposition, charge-discharge properties, cyclic voltammetry

1. Introduction

For decades, chromium coatings have been extensively used to protect machinery, decorative surfaces, and marine structures such as ship hulls. However, the use of chromium-based coatings has declined due to the carcinogenic nature of chromates and the high toxicity of electrolytes containing hexavalent chromium. As a result, researchers have sought safer and more environmentally friendly alternatives. Among them, tungsten has emerged as a promising candidate for developing advanced coatings, thanks to its excellent thermal conductivity, high corrosion resistance, and non-toxic characteristics. Despite these advantages, the high melting point of tungsten makes traditional alloy fabrication methods challenging. In cobalt matrices, the solubility of tungsten is limited to around 1 wt.% [1].To overcome these limitations, electrodeposition has been introduced as an effective method for incorporating tungsten into alloys, especially with iron-group metals like cobalt. The resulting Co–W alloys exhibit improved wear and corrosion resistance [2, 3]. Compared to molten metals, electrodeposited metals often show higher corrosion current densities and more negative corrosion potentials [4]. Additionally, semi-rigid Co–W alloys with 2–3 at.% tungsten content display ferromagnetic behavior, while coatings with higher tungsten content (approximately 30 at.%) tend to be softer and non-ferromagnetic, highlighting the importance of composition [5].

Since corrosion is a deteriorative process that limits the functional lifespan of metals and alloys, it is essential to develop corrosion-resistant materials [6]. Co–W alloys have found applications in gas turbines, jet engines, dies, valves, and tooling systems [7]. Their outstanding mechanical strength, tribological performance, and chemical stability make them promising to replace traditional chromium coatings [4, 8, 9]. Moreover, cobalt retains its magnetic properties when alloyed with less than 20% tungsten [10], enabling its use in magnetic thin films and disk memory devices [11-14].

Among the available techniques, electrodeposition stands out as a versatile, cost-effective, and scalable method for producing dense nanocrystalline coatings. It allows precise control over coating thickness, morphology, and composition [15-18]. The Co–W alloy system is a typical example of induced co-deposition [10, 19, 20], where tungsten, otherwise difficult to deposit, forms an alloy through co-deposition with iron-group metals. Although several mechanisms have been proposed to explain this phenomenon [21], the resulting alloys retain valuable functionality. One key property is nanocrystallinity, which influences both physical and electrochemical performance [22]. The tungsten content in Co–W coatings significantly affects their structural refinement, allowing effective deposition in deep features and complex geometries. Several strategies have been employed to improve mass transfer, including pulse plating [10, 23], increasing electrolyte temperature, and ultrasonic agitation [24]. Tungsten alloy coatings are typically produced using citric or gluconate-based electrolytes when paired with iron-group metals [13, 25].

Due to their mechanical robustness, magnetic performance, wear resistance, and conductivity, tungsten-based alloys are well-suited for harsh environments like ULSI barriers, aerospace components, and high-performance motors. In particular, Co–W coatings show potential in hydrogen purification, MEMS devices, and protective surface applications, providing properties comparable to hard chromium coatings [8, 14, 26-29].

The development of Co–W and W-based alloys with amorphous or nanostructured morphology continues to gain attention, as these materials exhibit high charge-discharge capacity and superior corrosion resistance in both acidic and alkaline media. The transition toward non-toxic coatings as alternatives to chromium has accelerated interest in tungsten–iron group alloys [30-33]. These materials combine excellent tribological, electrical, magnetic, and mechanical properties, along with high corrosion resistance across various environments [34, 35]. Their exceptional wear performance also supports their use in gas turbines, engines, dies, and valve systems [34], in addition to potential applications as electrodes for hydrogen evolution [35].

It is also worth noting that the economic and biocompatibility limitations of noble metals have renewed interest in chromium-based alloys, particularly in surgical applications. For example, Co–Cr surgical alloys often include 6–8 wt.% molybdenum, which enhances passivation, while 27% chromium content is typical for improving corrosion resistance [36, 37].

The unique properties of nanostructured materials, derived from their fine grain size, offer exciting opportunities for demanding applications [38]. Over the past two decades, several methods—such as hydrothermal-mechanical-chemical, hydrothermal-electrochemical, and electrodeposition techniques—have been developed to synthesize such materials [39]. Among these, electrodeposition remains the most practical, scalable, and cost-effective route for industrial adaptation. Today, global research efforts continue to explore various deposition strategies and bath compositions for the co-deposition of tungsten with iron-group metals, driven by the search for high-performance and sustainable coating solutions [38, 39].

This study focuses on the electrodeposition of Co, W, and Co–W coatings using galvanostatic and chronoamperometric techniques, with parameters optimized based on bath composition and deposition conditions. Prior studies have reported these coatings in amorphous, crystalline, and nanocrystalline forms, highlighting their adaptability to modern technologies.

2. Experimental

2.1. Materials and electrodes

All chemicals were of analytical grade and used as received without further purification. The chemicals used in this study include silver nitrate ($AgNO_3$, ≥99%, Sigma-Aldrich), potassium nitrate (KNO_3, ≥99%, BDH), cobalt(II) chloride hexahydrate ($CoCl_2 \cdot 6H_2O$, ≥98%, Sigma-Aldrich), potassium chloride (KCl, ≥99%, BDH), Sodium tungstate dihydrate ($Na_2WO_4 \cdot 2H_2O$, ≥99% purity, Sigma-Aldrich, citric acid ($C_6H_8O_7$, ≥99.5%, Merck), trisodium citrate dihydrate ($Na_3C_6H_5O_7 \cdot 2H_2O$, ≥99%, Sigma-Aldrich), and sodium tetraborate decahydrate (borax, $Na_2B_4O_7 \cdot 10H_2O$, ≥99%, BDH). Distilled water was used for all solution preparations.

The electrochemical experiments were conducted using a glassy carbon electrode with an exposed surface area of 1 cm^2 as the working substrate. Prior to each electrodeposition process, the substrate was mechanically polished to achieve a smooth surface, followed by thorough rinsing with distilled water. Immediately afterward, the electrode was placed into a three-electrode electrochemical cell for deposition.

The three-electrode system consisted of a saturated Ag/AgCl reference electrode, a platinum sheet as the counter electrode, and the glassy carbon electrode as the working electrode, which was modified with a silver layer supported on a copper base. All potentials reported are relative to the reference electrode.

The following steps were performed for substrate preparation and material deposition:

A) Substrate Preparation:

- Silver was electrodeposited onto the copper surface using cyclic voltammetry (multi-cycle scan), ranging from –0.1 V to +0.7 V in an electrolyte containing 0.005 M $AgNO_3$ and 0.1 M KNO_3.

B) Electrodeposition of Cobalt (Co):

- Conducted under optimized conditions with an electrolyte of 0.005 M $CoCl_2.6H_2O$ and 0.1 M KCl at pH 2.5.
- Chronoamperometry was applied at –1.4 V for 100 s, and galvanostatic deposition was performed at –2 mA for 100 s to produce a thin cobalt layer.

C) Electrodeposition of Tungsten (W):

- Performed under similar conditions as Co, using 0.005 M $(NH_4)_{10}W_{12}O_{41}.5H_2O$ and 0.1 M KCl at pH 2.5.
- The deposition was achieved using chronoamperometry at –1.4 V for 100 s and the galvanostatic method at –2 mA for 100 s.

D) Electrodeposition of Co–W Alloy:

- Conducted using a mixed electrolyte containing 0.005 M Co^{2+}, 0.005 M W^{6+}, 0.1 M citric acid, 0.1 M citrate, and 0.1 M borax, adjusted to pH 5.
- Co–W alloy coatings were deposited using both galvanostatic (-2 mA for 100 s) and chronoamperometric (–1.4 V for 100 s) techniques to form uniform thin films.

CO_2 was bubbled into the solution for approximately 30 minutes to achieve complete saturation, resulting in a stable pH of 3.5. This duration was determined to be optimal for ensuring consistent and reproducible acidification conditions.

All electrochemical depositions were carried out at room temperature, utilizing chronoamperometry and galvanostatic methods to achieve consistent and controlled coating morphology.

2.2. Charge–Discharge Studies of the Coatings

The charge–discharge performance of the coatings was evaluated through cyclic charge–discharge measurements conducted in an acidic medium (0.1 M H_2SO_4). The tests were performed at varying discharge current densities (0.01, 0.02, 0.03, 0.04, 0.05, and 0.1 $mA \cdot cm^{-2}$), with three consecutive cycles for each current setting. From these measurements, key electrochemical parameters, including discharge time (t_{dis}), specific capacitance (S.C., mAh), and specific energy density, were determined for all three types of electrode coatings under study.

3. Results and Discussion:

3.1. Preparation of coatings

In this study, a glassy carbon electrode (GCE) modified with a thin silver layer was employed as the working electrode to investigate the electrochemical deposition behavior of cobalt (Co), tungsten (W), and their binary alloy (Co–W). The silver layer was prepared via multi-cycle cyclic voltammetry in the potential range from –0.1 V to +0.7 V using an aqueous solution containing 0.005 M $AgNO_3$ and 0.1 M KNO_3. As shown in **Figure 1A**, the cyclic voltammogram clearly indicates the characteristic redox peaks corresponding to the electrodeposition of silver, confirming the successful formation of a silver coating on the GCE substrate.

Subsequent electrodeposition of cobalt was carried out under optimized conditions (0.005 M Co^{2+}, 0.1 M KCl, pH 2.5), employing both chronoamperometry at –1.4 V for 100 s (**Figure 1B**) and galvanostatic deposition at –2 mA for 100 s (**Figure 1C**). The current–time transient in 1B reflects a sharp initial cathodic current followed by stabilization, typical of nucleation and growth processes for thin Co films. The galvanostatic curve (1C) confirms a stable deposition regime under constant current.

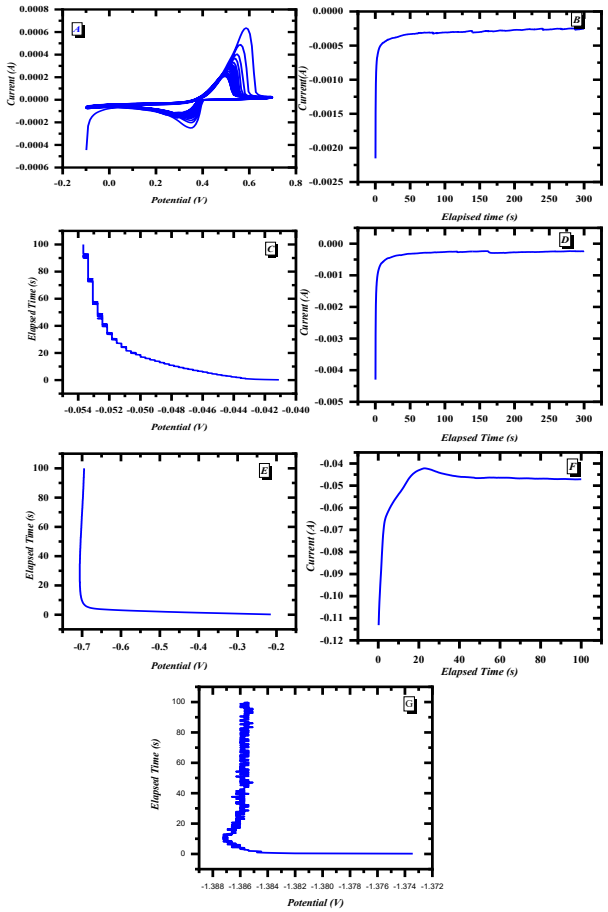

Fig.1. Electrodeposition of silver by multi-CVs (A), chrono amperometry method electrodeposition of Co (B), galvanostatic electrodeposition of Co (C), electrodeposition of W by chronoamperometry (D), electrodeposition of W by galvanostatic (E), electrodeposition of CoW by chronoamperometry (F), and Electrodeposition of CoW by galvanostatic (G).

Similarly, the deposition of tungsten was performed using identical electrochemical techniques and conditions (0.005 M W^{6+}, 0.1 M KCl, pH 2.5). The chronoamperometric plot for W deposition (**Figure 1D**) reveals a rapid current decay followed by a plateau, indicative of diffusion-limited deposition behavior. The corresponding galvanostatic curve (**Figure 1E**) maintains consistent current input with a gradually increasing potential, reflecting the increasing resistance at the growing metal–electrolyte interface.

For the Co–W alloy, a mixed electrolyte composed of 0.005 M Co^{2+}, 0.005 M W^{6+}, 0.1 M citric acid, 0.1 M citrate, and 0.1 M borax at pH 5 was used. Deposition was performed under chronoamperometric and galvanostatic modes. The chronoamperometric curve (**Figure 1F**) shows a smooth decrease in current density with time, indicative of concurrent co-deposition and stabilization of both metal species onto the electrode. The galvanostatic deposition of the alloy, shown in **Figure 1G**, demonstrates the potential profile required to sustain the applied current, with distinct features associated with the alloying process and intermetallic interactions.

Overall, the sequence of electrodeposition techniques confirms the successful synthesis of Co, W, and Co–W thin films on Ag-modified GCE. The combined use of chronoamperometry and galvanostatic methods enables precise control over layer thickness and composition, which is essential for tuning the physical and electrochemical properties of the resulting coatings. These procedures lay the foundation for subsequent characterization and performance evaluation of the fabricated electrodes.

3.2.Voltammetric study of carbon dioxide reduction

One promising path toward the sustainable production of valuable chemicals and fuels is electrochemical CO_2 reduction [40-43]. Voltammetric studies are carried out with and without CO_2. Figure 2 shows the voltammetric behavior of Ag, Co, W, and Co-W electrodeposited on the modified GCE with electrodeposited silver electrodes in the presence of CO_2. Reduction peak of CO_2 at the Ag electrode at a potential of -1.54 V. In the case of using CO, W, and Co-W alloy electrodes, the potential of the reduction peak has been shifted to a more positive direction, -1.31, -1.22, and -1.17 V, respectively. This behavior indicated that the electrodeposited layers on the GCE/Ag substrate enhanced and catalyzed the reduction process of the carbon dioxide. The above reduction peak potential values indicated that the Co-W alloy surface enhanced electrode performance in conditions favoring carbon dioxide reduction more than the other coatings. The results obtained for the electrodeposited Co, W, and Co-W alloy electrodes were compared with those from bare GCE/Ag electrodes, revealing that a high deposit of Co-W alloy shows greater current density during the reduction process of carbon dioxide.

In this regard, electrodeposition serves as an effective technique for fabricating coatings and catalysts. Its advantages include: (1) the ability to produce catalysts with uniform composition and strong substrate adhesion through controlled deposition parameters. For instance, it is simple to control electrodes, voltage, current density, electrolyte composition, etc.

(2). It is possible to create morphologically controlled nanostructures. (3) The procedure is straightforward, and the deposition conditions are convenient. The wide range of experimental parameters and the substrate's impact on the catalyst's shape and chemical makeup, however, are two major obstacles to electrodeposition. Figure 3 shows linear scan voltammetry, which has been carried out to confirm the behavior obtained from cyclic voltammetric studies for Co, W, and Co-W alloy electrodes in 0.1 M H_2SO_4.

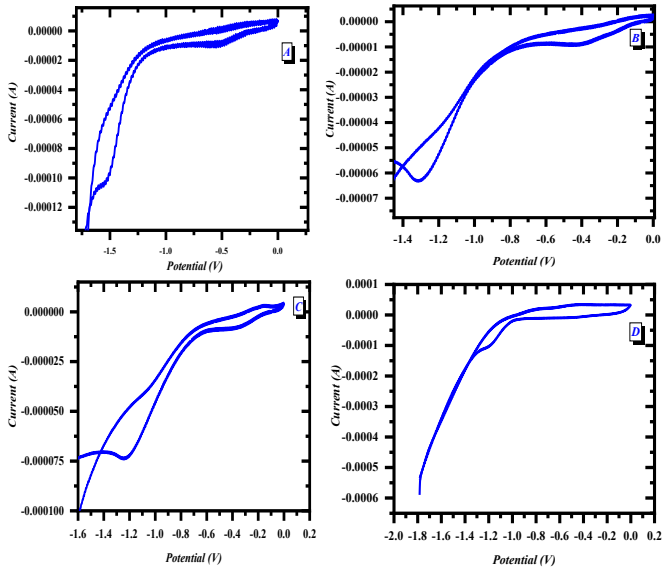

Fig. 2. Cyclic voltammograms recorded in CO_2 atmosphere at a scan rate of 0.05 $V \cdot s^{-1}$ for: (A) Ag electrode, (B) Co/Ag/GCE, (C) W/Ag/GCE electrode, and (D) Co-W/Ag/GCE electrode.

The mass diffusion rate and the accessibility of active sites are significantly influenced by the nature of the deposited layer, which makes it a significant factor in the carbon dioxide reduction reaction (CO_2RR).

Consequently, while limited efforts have been focused on the investigation of the deposited layer to optimize the electrodes' performance toward the CO_2RR, aforementioned alterations have been devoted to the production of cathode material with novel properties. The work mentioned above focuses on thoroughly examining the important electrode elements and how they affect the CO_2RR performance. The current density and the potential at which the reduction process took place are found to be greatly impacted by the deposited layers.

Co–W alloys exhibit a synergistic interaction where cobalt acts as an active center for CO_2 adsorption and intermediate stabilization, while tungsten adjusts the alloy's electronic structure, optimizing the d-band center and improving binding energies. This dual functionality facilitates better electron transfer and stabilization of reaction intermediates.

The electrochemical CO_2 reduction pathway likely follows the commonly proposed reactions **[40, 41]**:

$$CO_2 + 2H^+ + 2e^- \rightarrow CO + H_2O \quad (1)$$

$$CO_2 + H^+ + 2e^- \rightarrow HCOO^- \quad (2)$$

The presence of both Co and W enhances the likelihood of these reaction pathways by stabilizing key intermediates (*COOH or *HCOO) and lowering the activation energy.

Table 1 compares the CO_2 reduction potential values of the synthesized Co, W, and Co-W alloy electrodes with various materials reported in recent literature.

The Co-W alloy electrode in this study shows a reduction potential of –1.17 V, which is more positive (i.e., requires less overpotential) than both pure Co (–1.31 V) and W (–1.22 V) electrodes under identical conditions. Compared to other advanced catalysts like Ag-Co (–2.0 V), Ag/Co-MOF (–1.8 V), and Co_3O_4 nanofibers (–1.5 V), the Co-W alloy demonstrates a significantly improved (less negative) reduction potential. This suggests better catalytic efficiency for CO_2 reduction, as lower overpotential typically correlates with enhanced activity. While Cu-CF_2 (–1.4 V) and other Ag-based systems are traditionally used for CO_2 electroreduction, they suffer from relatively high overpotentials and stability issues. In contrast, the Co-W alloy offers a promising balance of activity and potential stability, potentially due to synergistic interactions between Co and W atoms, which may facilitate faster electron transfer and more favorable adsorption/desorption of CO_2 intermediates.

Table 1. Comparison of the CO_2 reduction potential values for Co, W, and Co-W alloy with recent studies.

Electrode	Reduction potential (V)	Reference
Cu-CF_2	-1.4	[44]
Co_3O_4 nanofibers	-1.5	[45]
Ag-Co	-2	[46]
Ag/Co- MOF	-1.8	[47]
Co-W @GCE/Ag	-1.17	This work
Co @GCE/Ag	-1.31	This work
W @GCE/Ag	-1.22	This work

3.3.Charge-discharge studies

The pursuit of efficient and long-lasting energy storage systems is a driving force in the evolution of modern energy technologies. One such avenue involves the exploration of electrochemical supercapacitors (SCs), which hold great promise as high-power devices capable of delivering fast energy bursts and withstanding numerous charge–discharge cycles without significant degradation **[42-47].** Supercapacitors effectively bridge the gap between conventional dielectric capacitors and batteries, combining high power densities with moderate energy densities. However, several challenges persist, especially in achieving the high specific energy required for extended applications such as electric vehicles, portable electronics, and backup systems. The core strategy to overcome these challenges involves enhancing the specific capacitance and energy density of the electrode materials while maintaining high cycle stability and conductivity.

In this study, the electrochemical charge–discharge behavior of cobalt (Co), tungsten (W), and cobalt–tungsten (Co–W) alloy coatings—each electrodeposited onto silver-modified glassy carbon electrodes—was systematically examined in 0.1 M sulfuric acid (H_2SO_4) using the galvanostatic charge–discharge method. The electrodes were tested under different applied current densities ranging from 0.01 to 0.1 $mA \cdot cm^{-2}$. Key performance indicators such as discharge time (t_{dis}), specific

capacitance (S.C., in F/g), and specific energy density (E_{sp}, in J/kg) were calculated to evaluate the performance of each electrode configuration. Findings from this section offer a deep understanding of how composition and electrochemical parameters affect the performance of electrode materials in acidic environments.

To establish a baseline, the galvanostatic charge–discharge (GCD) profiles of the Ag-modified electrodes were first evaluated at 0.01 mA·cm^{-2} (Figure 3). The nearly symmetric triangular profiles of the charge–discharge curves in Figure 3 (A–D) suggest ideal capacitive behavior, characterized by low internal resistance and high coulombic efficiency, indicative of reversible charge storage processes. Among the tested electrodes, the Co-modified Ag electrode (Ag@Co, Figure 3B) demonstrated the longest discharge time, followed by Ag@Co–W (Figure 3D), Ag@W (Figure 3C), and the bare Ag electrode (Figure 3A). This suggests that the Co layer facilitates faradaic charge storage reactions, which contribute to enhanced capacitance. The Co-W alloy also showed promising behavior, benefiting from the synergy between cobalt's pseudocapacitance and tungsten's stability and conductivity.

A more detailed investigation was performed by studying the cycling behavior of each material across six different current densities, from 0.01 mA·cm^{-2} up to 0.1 mA·cm^{-2}. Figures 4 through 6 present the GCD curves for Co, W, and Co–W electrodes, respectively, and their corresponding numerical results are summarized in Tables 1, 2, and 3. These data allow for an in-depth comparison of how each electrode material performs under increasing current load.

Starting with cobalt (Co), Figure 4 illustrates the evolution of the GCD curves at rising current densities. At the lowest current density of 0.01 mA·cm^{-2} (Figure 4A), the discharge time (t_{dis}) reached a maximum of 75 seconds, with a stable voltage range (ΔV) of 0.5 V, yielding a specific capacitance of 4.06 F/g and energy density of 0.51 J/kg (Table 2). As current density increased, the discharge time declined sharply to 10 seconds at 0.1 mA·cm^{-2}, though interestingly, the specific capacitance increased again to 5.42 F/g at this current, suggesting that higher currents activate more electroactive sites or enhance ion transport kinetics in the Co layer. This non-monotonic behavior points to the complex interplay between current density, electroactive surface area, and redox reaction kinetics in the electrode material. The energy density also rose to 0.68 J/kg, making Co the most capacitive electrode among those tested.

In contrast, the behavior of tungsten (W) electrodes (Figure 5) followed a different trend. At 0.01 mA·cm^{-2}, the W electrode displayed a higher operating voltage of 0.9 V and achieved a specific energy density of 2.49 J/kg, the highest among all electrodes (Table 3). However, its specific capacitance was higher than Co's, measured at 6.17 F/g. As the current density increased to 0.1 mA·cm^{-2}, the W electrode showed a modest increase in capacitance to 11.39 F/g, and the energy density at this point was 2.41 J/kg. These findings suggest that while W may not support as many faradaic reactions as Co, its ability to maintain a broad voltage window enables it to store more energy overall. This makes W a suitable material for applications where energy density is prioritized over charge storage rate.

The cobalt–tungsten (Co–W) alloy electrodes exhibited an intermediate behavior, combining features from both parent metals. As seen in Figure 6, at low current density (0.01 mA·cm^{-2}), Co–W had a discharge time of 75 seconds, a voltage range of 0.5 V, a specific capacitance of 8.63 F/g, and an energy density of 1.55 J/kg (Table 4). As current increased, the performance initially declined, with a dip in both tdis and S.C., reaching a minimum at around 0.03–0.05 mA·cm^{-2}. However, at 0.1 mA·cm^{-2}, the Co–W alloy electrode regained performance, recording a specific capacitance of 7.77 F/g and an energy density of 0.97 J/kg. This resurgence can be attributed to improved ion accessibility or microstructural activation of the alloy at higher current stresses. The Co–W alloy thus provides a high balance, offering both reasonable capacitance and energy density, and may be more chemically and mechanically stable than pure Co under prolonged operation.

Comparing all materials at 0.1 mA·cm^{-2}, the specific capacitance order was observed as:
Co (5.42 F/g) < Co–W (8.63 F/g) < W (11.39 F/g) **[39, 48]**

Whereas, the specific energy density order was:
W (2.41 J/kg) > Co–W (1.55 J/kg) > Co (0.68 J/kg)

These findings reveal an interesting inverse relationship: materials with higher capacitance (e.g., Co) do not necessarily yield higher energy densities, which are also dependent on the voltage window as shown in the energy density equation $E=1/2CV^2$. Since voltage appears in squared form, a material with a broader potential window (like W) can compensate for lower capacitance and still deliver greater energy **[49-51].**

Moreover, the performance of all electrodes was measured in an aqueous H_2SO_4 electrolyte, which generally limits the maximum potential window due to water decomposition (typically around 0.6–0.7 V). Despite this limitation, the results demonstrate the ability of the selected electrode materials to perform efficiently within this electrochemical stability range. In future studies, switching to non-aqueous or hybrid electrolytes could further boost voltage and energy density. From a design perspective, the development of thick electrodes with high areal capacity is crucial for real-world supercapacitor systems, especially when optimizing for volume- or mass-based energy storage. However, this comes with challenges such as maintaining conductivity, electrolyte accessibility, and long-term mechanical integrity under repeated cycling. The Co–W alloy may offer advantages here, due to its ability to combine the pseudocapacitive nature of cobalt with the robustness of tungsten. This comparative charge–discharge study illustrates that each material presents unique benefits: cobalt is favorable for high specific capacitance, tungsten excels in energy density, and the Co–W alloy delivers a balanced performance suitable for multifunctional energy storage applications **[52-54].** These findings can inform the strategic selection or design of electrode materials for next-generation supercapacitors that aim to optimize both power and energy delivery while maintaining stability and environmental sustainability.

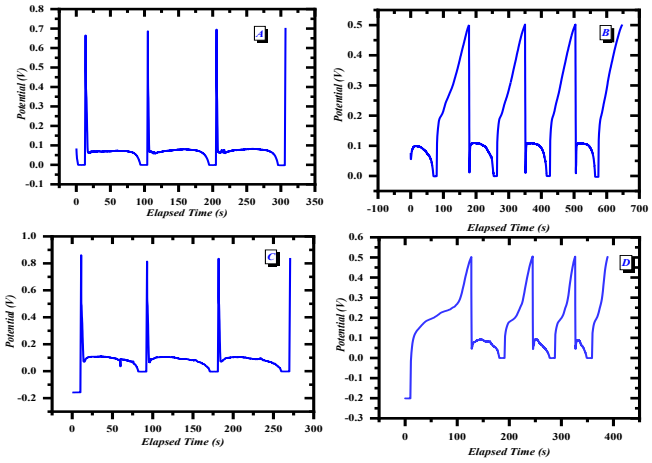

Fig. 3. Charge-discharge of Ag electrode (A), Ag@Co (B), Ag@W (C), charge–discharge of Ag @Co-W (D) at applied current density of 0.01 mA. cm^{-2} in 0.1 M H_2SO_4 solution.

Table 2. Charge discharge parameters obtained for Co electrodeposited by chronoamperometry in 0.1 M H_2SO_4 solution at different applied current densities.

Applied current density mA. cm^{-2}	t_{dis} (s)	ΔV (V)	*S.C.* (F /g)	$E_{s.p}$ (J /g)
0.01	75	0.9	6.17	2.49
0.02	25	0.6	6.17	1.11
0.03	20	0.6	6.84	1.23
0.04	10	0.65	4.55	0.96
0.05	15	0.6	9.25	1.66
0.1	10	0.65	11.39	2.41

Table 3. Charge discharge parameters obtained for W electrodeposited by chronoamperometry in 0.1 M H_2SO_4 solution at different applied current densities.

Applied current density mA. cm^{-2}	t_{dis} (s)	ΔV (V)	*S.C.* (F /g)	$E_{s.p}$ (J /g)
0.01	75	0.5	7.77	0.97
0.02	20	0.5	4.14	0.52
0.03	10	0.55	2.82	0.43
0.04	10	0.55	3.77	0.58
0.05	10	0.55	4.71	0.71
0.1	10	0.60	8.63	1.55

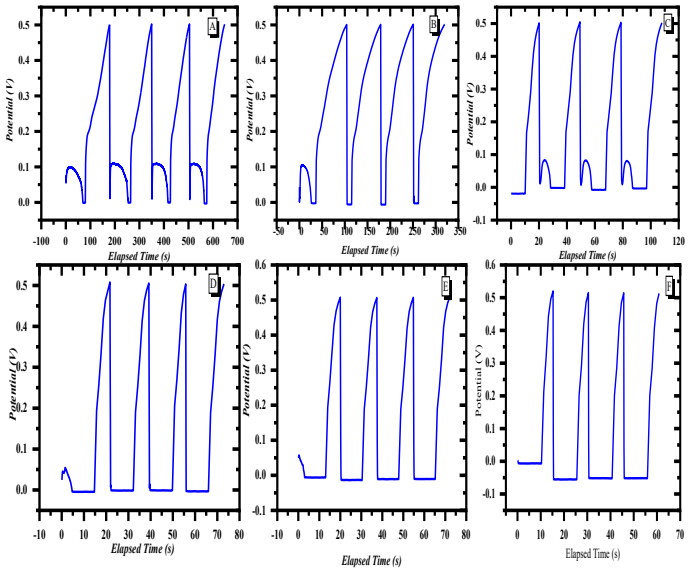

Fig. 4. Charge-discharge cycling curves of Co at an applied current density of 0.01mA.cm^{-2} (A), 0.02 mA.cm^{-2} (B), 0.03 mA.cm^{-2} (C), 0.04 mA.cm^{-2} (D), 0.05 mA.cm^{-2} (E), 0.1 mA.cm^{-2} (F) in 0.1 M H_2SO_4 solution.

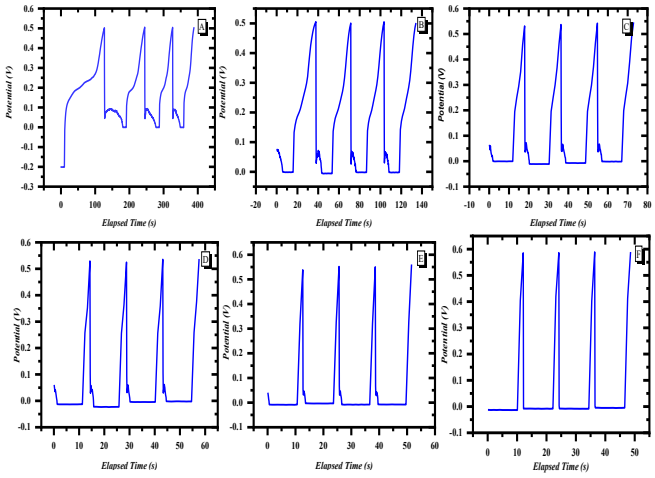

Fig. 5. Charge-discharge cycling curves of W at an applied current density of 0.01mA.cm^{-2} (A), 0.02 mA.cm^{-2} (B), 0.03 mA.cm^{-2} (C), 0.04 mA.cm^{-2} (D), 0.05 mA.cm^{-2} (E), 0.1 mA.cm^{-2} (F) in 0.1 M H_2SO_4 solution.

Table 4. Charge discharge parameters obtained for Co-W electrodeposited by chronoamperometry in 0.1 M H_2SO_4 solution at different applied current densities.

Applied current density (mA. cm^{-2})	t_{dis} (s)	ΔV (V)	*S.C.* (F /g)	$E_{s.p}$ (J / g)
0.01	75	0.5	4.06	0.51
0.02	25	0.5	2.71	0.34
0.03	20	0.5	3.25	0.41
0.04	10	0.5	2.16	0.27
0.05	10	0.5	2.71	0.34
0.1	10	0.5	5.42	0.68

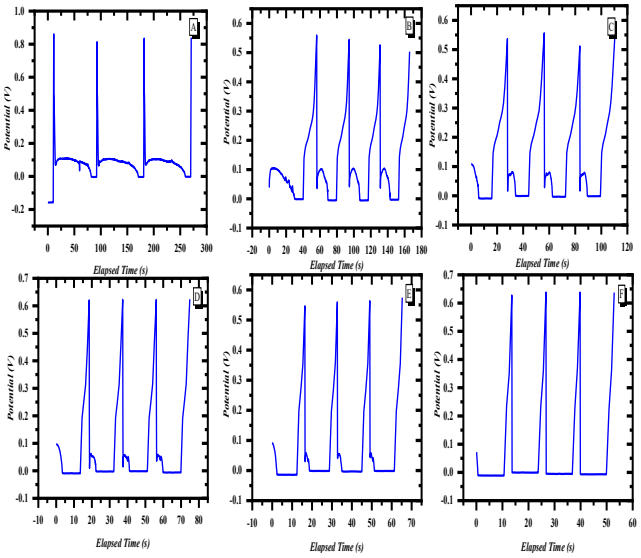

Fig. 6. Charge-discharge cycling curves of Co-W at an applied current density of 0.01mA.cm^{-2} (A), 0.02 mA.cm^{-2} (B), 0.03 mA.cm^{-2} (C), 0.04 mA.cm^{-2} (D), 0.05 mA.cm^{-2} (E), 0.1 mA.cm^{-2} (F) in 0.1 M H_2SO_4 solution.

Table 5 presents quantitative measurements of the mass and thickness of Co, W, and Co–W alloy coatings obtained by electrodeposition, offering experimental validation of the deposition process. These measurements are critical in confirming that the electrodeposition parameters successfully produced distinguishable and controlled layers with varied morphologies and material characteristics.

The pure Co deposit shows the greatest thickness (41.5 µm) and mass (0.000369 g), indicating a relatively high deposition rate and possibly more porous or loosely packed growth. In contrast, pure W, known for its challenging electrodeposition behavior, resulted in significantly lower mass (0.000135 g) and reduced thickness (7.02 µm), consistent with literature on its limited deposition efficiency.

Most notably, the Co–W alloy deposit exhibited **an** intermediate mass (0.000193 g) but a very low thickness (1.721 µm), strongly suggesting the formation of a denser, more compact film. This aligns with the hypothesis that alloying modifies the nucleation and growth mechanisms, promoting the development of highly adherent, fine-grained structures.

Table 5. Mass and Thickness of Co, W, and Co-W alloy deposits.

Metal /Alloy	Co	W	Co-W alloy
Mass (g)	0.000369	0.000135	0.000193
Thickness (µm)	41.5	7.02	1.721

Table 6 presents a comparative analysis of the specific capacitance values for Co, W, and Co–W alloy electrodes evaluated in this study, alongside values from recent literature for similar materials. The Co–W alloy electrode synthesized in this work exhibits a specific capacitance of 7.77 F/g, which is significantly higher than the values reported for other materials such as WCF/CAG (1.4 F/g), WCF/CuO (0.33 F/g), and WCF/CAG (0.212 F/g). The enhanced performance of Co–W over the individual Co (4.06 F/g) and W (6.17 F/g) electrodes confirms a synergistic effect between the two metals, likely improving electronic conductivity, surface redox activity, and charge storage behavior. Compared to the literature, the performance boost in this study could also be attributed to the nano-structuring of the electrode surface and uniform alloy dispersion, which enhance electrolyte accessibility and active surface area.

Table 6. Comparison of Specific Capacitance of Co and W and Co-W alloy with recent studies.

Electrode	Specific capacitance (F/g)	Reference
WCF/CAG	1.4	[55]
WCF/CuO	0.33	[55]
WCF/CAG	0.212	[56]
CF/CAG	1.49	[57]
Co-W @GCE/Ag	7.77	This work
Co @GCE/Ag	4.06	This work
W @GCE/Ag	6.17	This work

The multifunctional behavior of the Co–W alloy electrode arises from its unique structural and electronic properties, which support both catalytic and charge storage processes. Scientifically, the Co component facilitates CO_2 adsorption and activation due to its moderate binding energy with CO_2 intermediates, while W modulates the electronic structure and improves conductivity and surface stability. This synergy not only enhances CO_2RR efficiency but also benefits supercapacitor behavior through increased surface area and redox-active sites, which are essential for pseudocapacitive storage.

In both applications, the electrochemical reactions rely on accessible active sites, fast charge transfer, and stability under varying potential regimes. The Co–W alloy's nanostructured morphology and mixed valence states (e.g., Co^{2+}/Co^{3+}) enable it

to store charge reversibly and simultaneously offer catalytic sites for CO_2 conversion. Therefore, the same electrode can potentially switch between energy storage and catalytic modes, particularly in hybrid devices or integrated systems. Further research is ongoing to investigate the long-term cycling and real-time performance under dual-function conditions.

4. Conclusion

This study explored the electrochemical and energy storage properties of electrodeposited Co, W, and Co-W alloy coatings on Ag-modified glassy carbon electrodes. CO_2 reduction experiments using cyclic and linear scan voltammetry revealed a positive shift in reduction peak potentials with Co, W, and particularly Co-W coatings, indicating enhanced catalytic activity toward CO_2 electroreduction (CO_2RR). The Co-W alloy showed the most favorable performance, attributed to synergistic effects between cobalt and tungsten that improve electron transfer and CO_2 adsorption. Increased current density further supported the alloy's superior catalytic efficiency. These results suggest that nanostructured Co-W alloys are promising, environmentally benign electrocatalysts for CO_2 conversion. In parallel, charge-discharge tests in 0.1 M H_2SO_4 highlighted the energy storage potential of the same materials. Cobalt coatings achieved the highest specific capacitance due to their efficient faradaic charge transfer, while tungsten exhibited the highest energy density, likely due to a broader potential window. The Co-W alloy provided balanced performance, combining moderate capacitance and energy density, which makes it suitable for multifunctional applications. Overall, the study demonstrates that electrodeposited Co–W coatings offer dual functionality, effective CO_2RR catalysis, and competitive energy storage, positioning them as promising candidates for integrated electrochemical systems such as CO_2-utilizing energy devices. Future work should aim to optimize alloy composition, microstructure, and operational stability to further enhance their practical applicability.

CRediT authorship contribution statement:

Mahmoud Elrouby: Conceptualization, Methodology, writing-original draft, Review & Editing, Supervision of data collection.
Hoda Abdel Shafy Shilkamy: Methodology, Writing-Original draft, Review & Editing, supervision.
Hossnia S. Moharan: Review, General Supervision.
Eman Ragab: Data collection, Data analysis, writing contribution, and data processing. All authors have read and agreed to the published version of the manuscript.

Data availability statement

The data used to support the findings of this study are available from the corresponding author upon request.

Declaration of Competing Interest

The authors declare that they have no known competing financial interests or personal relationships that could have appeared to influence the work reported in this paper.

Acknowledgments

The authors gratefully acknowledge the support of [Sohag University/ Chemistry Department], as well as the contributions of colleagues who provided insights and feedback during the development of this research.

References

[1] S. Dulal, C.B. Shin, J.Y. Sung, C.-K. Kim, *Journal of Applied Electrochemistry*, 38, (2008) 83-91.
[2] Y.S. Yapontseva, A. Dikusar, V. Kyblanovskii, *Surface Engineering and Applied Electrochemistry*, 50, (2014) 330-336.
[3] H. Capel, P. Shipway, S. Harris, *Wear*, 255, (2003) 917-923.
[4] N. Tsyntsaru, H. Cesiulis, E. Pellicer, J.-P. Celis, J. Sort, *Electrochimica Acta*, 104, (2013) 94-103.
[5] E. Vernickaite, N. Tsyntsaru, H. Cesiulis, *Surface and Coatings Technology*, 307, (2016) 1341-1349.
[6] S. Mayanna, L. Ramesh, B. Maruthi, D. Landolt, *Journal of Materials Science Letters*, 16, (1997) 1305-1306.
[7] D. Weston, P. Shipway, S. Harris, M. Cheng, *Wear*, 267, (2009) 934-943.
[8] N. Tsyntsaru, *Russian Journal of Electrochemistry*, 52, (2016) 1041-1047.
[9] Z. Ghaferi, K. Raeissi, M. Golozar, H. Edris, *Surface and Coatings Technology*, 206, (2011) 497-505.
[10] N. Tsyntsaru, H. Cesiulis, M. Donten, J. Sort, E. Pellicer, E.J. Podlaha-Murphy, *Surface Engineering and Applied Electrochemistry*, 48, (2012) 491-520.
[11] U. Admon, M. Dariel, E. Grunbaum, J. Lodder, *Journal of applied physics*, 62, (1987) 1943-1947.
[12] N.V. Myung, D.-Y. Park, B.-Y. Yoo, P.T. Sumodjo, *Journal of magnetism and magnetic materials*, 265, (2003) 189-198.
[13] H.H. Yang, N. Myung, J. Yee, D.-Y. Park, B.-Y. Yoo, M. Schwartz, K. Nobe, J.W. Judy, *Sensors and Actuators A: Physical*, 97, (2002) 88-97.
[14] N. Sulitanu, *Journal of Magnetism and Magnetic Materials*, 231, (2001) 85-93.
[15] L. Rodríguez-Sánchez, M.C. Blanco, M.A. López-Quintela, *The Journal of Physical Chemistry B*, 104, (2000) 9683-9688.
[16] N.R.N. Masdek, Z. Salleh, M.H. Koay, M.A. Ismail, IOP Conference Series: *Materials Science and Engineering*, 380, (2018) 012012.
[17] S. Domínguez-Domínguez, J. Arias-Pardilla, Á. Berenguer-Murcia, E. Morallón, D. Cazorla-Amorós, *Journal of Applied Electrochemistry*, 38, (2008) 259-268.
[18] S. Caporali, P. Marcantelli, C. Chiappe, C.S. Pomelli, *Surface and Coatings Technology*, 264, (2015) 23-31.
[19] Z. Galikova, M. Chovancova, V. Danielik, *Chemical Papers*, 60, (2006) 353-359.
[20] S. Belevskii, S. Yushchenko, A. Dikusar, *Surface Engineering and Applied Electrochemistry*, 45, (2009) 446-454.
[21] S. Belevskii, N. Tsyntsaru, A. Dikusar, *Surface Engineering and Applied Electrochemistry*, 46, (2010) 91-99.
[22] M.E. Hyde, R.G. Compton, *Journal of Electroanalytical Chemistry*, 531, (2002) 19-24.
[23] A. Ramazani, M.A. Kashi, M. Alikhani, S. Erfanifam, *Materials Chemistry and Physics*, 112, (2008) 285-289.
[24] Z.A. Hamid, *Materials Letters*, 57, (2003) 2558-2564.
[25] H.H. Yang, N.V. Myung, J. Yee, D.Y. Park, B.Y. Yoo, M. Schwartz, K. Nobe, J.W. Judy, *Sensors and Actuators A: Physical*, 97, (2002) 88-97.
[26] N.-T. Nguyen, X. Huang, T.K. Chuan, J. *Fluids Eng*., 124, (2002) 384-392.
[27] C.-M. Ho, Y.-C. Tai, *Annual review of fluid mechanics*, 30, (1998) 579-612.

[28] N. Tsyntsaru, *Russian Journal of Electrochemistry*, 52, (2016) 1041-1047.
[29] Y.S. Al Jabbari, *The journal of advanced prosthodontics*, 6, (2014) 138.
[30] S. Mercieca, M. Caligari Conti, J. Buhagiar, J. Camilleri, *Journal of applied biomaterials & functional materials*, 16, (2018) 47-54.
[31] X. Nan, F. Wang, S. Xin, X. Zhu, Q. Zhou, *Coatings*, 13, (2023) 665.
[32] D.W. Ernst, M.L. Holt, *Journal of The Electrochemical Society, 105, (1958) 686.*
[33] G. Yar-Mukhamedova, M. Ved, N. Sakhnenko, T. Nenastina, *Applied Surface Science*, 445, (2018) 298-307.
[34] M. Metikoš-Huković, Z. Pilić, R. Babić, D. Omanović, *Acta Biomaterialia*, 2, (2006) 693-700.
[35] O. Öztürk, U.u. Türkan, A.E. Erogˇlu, *Surface and Coatings Technology*, 200, (2006) 5687-5697.
[36] B. Lohberger, N. Eck, D. Glaenzer, H. Lichtenegger, L. Ploszczanski, A. Leithner, *Materials*, 13, (2020) 4292.
[37] N. Eliaz, E. Gileadi, Induced Codeposition of Alloys of Tungsten, Molybdenum and Rhenium with Transition Metals, in: C.G. Vayenas, R.E. White, M.E. Gamboa-Aldeco (Eds.) *Modern Aspects of Electrochemistry*, Springer New York, New York, NY, 2008, pp. 191-301.
[38] N. Tsyntsaru, H. Cesiulis, M. Donten, J. Sort, E. Pellicer, E.J. Podlaha-Murphy, *Surface Engineering and Applied Electrochemistry*, 48, (2012) 491-520.
[39] A.E.-R. El-Sayed, H.A.E.-S. Shilkamy, M. Elrouby, *International Journal of Hydrogen Energy*, 56, (2024) 418-431.
[40] Gattrell, M., N. Gupta, and A. Co, A review of the aqueous electrochemical reduction of CO2 to hydrocarbons at copper. *Journal of Electroanalytical Chemistry*, 2006. 594(1): p. 1-19.
[41] Li, D., et al., How to go beyond C 1 products with electrochemical reduction of CO 2. *Sustainable Energy & Fuels*, 2021. 5(23): p. 5893-5914.
[42] A. Bansode, A. Urakawa, *Journal of Catalysis*, 309, (2014) 66-70.
[43] M. Jitaru, D.A. Lowy, M. Toma, B.C. Toma, L. Oniciu, *Journal of Applied Electrochemistry*, 27, (1997) 875-889.
[44] Chang, Q., et al., Electrochemical CO_2 Reduction Reaction over Cu Nanoparticles with Tunable Activity and Selectivity Mediated by Functional Groups in Polymeric Binder. *JACS Au*, 2(1), (2022) 214-222.
[45] Aljabour, A., et al., Nanofibrous cobalt oxide for electrocatalysis of CO2 reduction to carbon monoxide and formate in an acetonitrile-water electrolyte solution. *Applied Catalysis B: Environmental*, 229, (2018) 163-170.
[46] Bernal, M., et al., CO2 electroreduction on copper- cobalt nanoparticles: *Size and composition effect. Nano Energy*, 53, (2018) 27-36.
[47] Zhang, S.-Y., et al., Ag-doped Co_3O_4 catalyst derived from heterometallic MOF for syngas production by electrocatalytic reduction of CO_2 in water. *Journal of Solid State Chemistry*, 263, (2018) 44-51.
[48] J. Li, M. Zhu, Y.-F. Han, *ChemCatChem*, 13, (2021) 514-531.
[49] R. Pachaiappan, S. Rajendran, P. Senthil Kumar, D.-V.N. Vo, T. K.A. Hoang, *Chemical Engineering Research and Design*, 177, (2022) 304-320.
[50] H. Shen, X. Yang, J. Song, H. Gao, Z. Wu, J. Yu, W. Lei, J. Yang, G. He, Q. Hao, *Journal of Solid State Electrochemistry*, 26, (2022) 353-363.
[51] S.L. Jadhav, A.L. Jadhav, P.B. Sarawade, B.K. Mandlekar, A.V. Kadam, *Journal of Energy Storage*, 82, (2024) 110540.
[52] X.-J. Ma, L.-B. Kong, W.-B. Zhang, M.-C. Liu, Y.-C. Luo, L. Kang, *Electrochimica Acta*, 130, (2014) 660-669.
[53] R. Chen, Z. Xu, Y. Xu, T. Lei, D. Liu, C. Chen, W. Wang, I. Zhitomirsky, M. Qu, G. Zhang, *Materials*, 18, (2025) 80.
[54] H.M.A. El-Lateef, M. Elrouby, H.A. El-Shafy Shilkamy, A. El-Rahman El-Sayed, *ChemElectroChem*, 11, (2024) e202300812.
[55] Muñoz, B.K., et al., Electrochemical comparison of 2D-flexible solid-state supercapacitors based on a matrix of PVA/H3PO4. *Polymers,* 15(20), (2023) 4036.
[56] Pernice, M.F., et al., Mechanical, electrochemical and multifunctional performance of a CFRP/carbon aerogel structural supercapacitor and its corresponding monofunctional equivalents. *Multifunctional Materials*, 5(2), (2022) 025002.
[57] Qian, H., et al., Multifunctional Structural Supercapacitor Composites Based on Carbon Aerogel Modified High Performance Carbon Fiber Fabric. *ACS Applied Materials & Interfaces*, 5(13), (2013) 6113-6122.